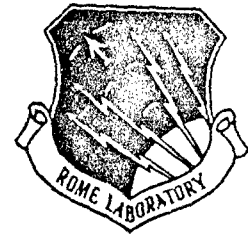


20030227103

AD-A266 128



RL-TR-93-42  
In-House Report  
April 1993



# ULTRA-LOW DENSITY AEROGEL MIRROR SUBSTRATES

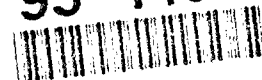
S. P. Hotaling

DTIC  
ELECTE  
JUN 23 1993  
S E D

APPROVED FOR PUBLIC RELEASE; DISTRIBUTION UNLIMITED.

03 6 22 083

93-14053



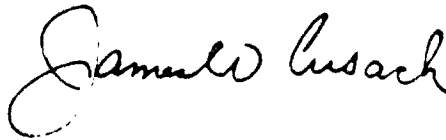
34128

Rome Laboratory  
Air Force Materiel Command  
Griffiss Air Force Base, New York

This report has been reviewed by the Rome Laboratory Public Affairs Office (PA) and is releasable to the National Technical Information Service (NTIS). At NTIS it will be releasable to the general public, including foreign nations.

RL-TR-93-42 has been reviewed and is approved for publication.

APPROVED:



JAMES W. CUSACK, Chief  
Photonics & Optics Division  
Surveillance and Photonics Directorate

FOR THE COMMANDER:



JAMES W. YOUNGBERG, LtCol, USAF  
Deputy Director  
Surveillance and Photonics Directorate

If your address has changed or if you wish to be removed from the Rome Laboratory mailing list, or if the addressee is no longer employed by your organization, please notify RL (OCPC) Griffiss AFB NY 13441-5700. This will assist us in maintaining a current mailing list.

Do not return copies of this report unless contractual obligations or notices on a specific document require that it be returned.

# REPORT DOCUMENTATION PAGE

Form Approved  
OMB No. 0704-0188

Public reporting burden for this collection of information is estimated to average 1 hour per response, including the time for reviewing instructions, searching existing data sources, gathering and maintaining the data needed, and completing and reviewing the collection of information. Send comments regarding this burden estimate or any other aspect of this collection of information, including suggestions for reducing this burden, to Washington Headquarters Services, Directorate for Information Operations and Reports, 1215 Jefferson Davis Highway, Suite 1204 Arlington, VA 22202-4302, and to the Office of Management and Budget, Paperwork Reduction Project (0704-0188), Washington, DC 20503.

1. AGENCY USE ONLY (Leave Blank)		2. REPORT DATE April 1993		3. REPORT TYPE AND DATES COVERED In-House Apr 90 - Sep 92	
4. TITLE AND SUBTITLE ULTRA-LOW DENSITY AEROGEL MIRROR SUBSTRATES				5. FUNDING NUMBERS PE - 62702F PR - 4506 TA - 15 WU - TK	
6. AUTHOR(S) S. P. Hotaling					
7. PERFORMING ORGANIZATION NAME(S) AND ADDRESS(ES) Rome Laboratory (OCPC) 25 Electronic Parkway Griffiss AFB NY 13441-4515				8. PERFORMING ORGANIZATION REPORT NUMBER RL-TR-93-42	
9. SPONSORING/MONITORING AGENCY NAME(S) AND ADDRESS(ES) Rome Laboratory (OCPC) 25 Electronic Parkway Griffiss AFB NY 13441-4515				10. SPONSORING/MONITORING AGENCY REPORT NUMBER	
11. SUPPLEMENTARY NOTES Rome Laboratory Project Engineer: S. P. Hotaling/OCPC (315) 330-3147					
12a. DISTRIBUTION/AVAILABILITY STATEMENT Approved for public release; distribution unlimited.				12b. DISTRIBUTION CODE	
13. ABSTRACT (Maximum 200 words) Despite the extremely low density and the hence low weight of aerogel materials, the applicability of these materials to reflective applications has had little attention due to the high porosities exhibited by the materials. This high porosity yields an intrinsically rough but uniform surface topology for aerogel of density in the low hundreds of milligrams per cubic centimeter and a fractal surface geometry for lower density aerogel (densities of the order of tens of milligrams per cubic centimeter). This paper presents new results of aerogel materials used as ultra-light substrates for reflective coatings by way of surface machining, polishing and planarization prior to metallization, and the optical characterization thereof. This paper presents a significant advance in the ability to polish and subsequently apply a thin film coating to low density aerogel materials, thus yielding ultra lightweight mirrors. The effects of ionizing radiation upon the aerogel heterostructures are found to be remarkably minimal up to a threshold of 35 Mrad y-ray irradiation. An exponential correlation was found to predict radiation effects at high y-doses.					
14. SUBJECT TERMS aerogel, optics, radiation effects, mirrors				15. NUMBER OF PAGES 38	
				16. PRICE CODE	
17. SECURITY CLASSIFICATION OF REPORT UNCLASSIFIED		18. SECURITY CLASSIFICATION OF THIS PAGE UNCLASSIFIED		19. SECURITY CLASSIFICATION OF ABSTRACT UNCLASSIFIED	
				20. LIMITATION OF ABSTRACT U/L	

## PREFACE

This paper was presented at the High Power Optical Components Conference (HIPOC) held at the National Institute of Standards Technology in Boulder Colorado. The conference was sponsored by the Strategic Defense Initiative Organization and was organized by the Naval Air Warfare Center (NAWC), China Lake, CA and W.J. Shaffer Associates. The conference proceedings are available from the NAWC (Weapons Division).

Accession For	
NTIS CRA&I	<input checked="" type="checkbox"/>
DTIC TAB	<input type="checkbox"/>
Unannounced	<input type="checkbox"/>
Justification .....	
By .....	
Distribution /	
Availability Codes	
Dist	Avail and / or Special
A1	

DTIC QUALITY INSPECTED 2

# ULTRA-LOW DENSITY AEROGEL MIRROR SUBSTRATES

S.P. HOTALING

Rome Laboratory/OCPC  
25 ELECTRONIC PKY  
GRIFFISS AFB, NY 13441-4515

*Despite the extremely low density and the hence low weight of aerogel materials, the applicability of these materials to reflective applications has had little attention due to the high porosities exhibited by the materials. This high porosity yields an intrinsically rough but uniform surface topology for aerogel of density in the low hundreds of milligrams per cubic centimeter and a fractal surface geometry for lower density aerogel (densities of the order of tens of milligrams per cubic centimeter). This paper presents new results of aerogel materials used as ultra-light substrates for reflective coatings by way of surface machining, polishing and planarization prior to metalization, and the optical characterization thereof. This paper represents a significant advance in the ability to polish and subsequently apply a thin film coating to low density aerogel materials, thus yielding ultra light weight mirrors. The effects of ionizing radiation upon the aerogel heterostructures are found to be remarkably minimal up to a threshold of 35 Mrad  $\gamma$ - ray irradiation. An exponential correlation was found to predict radiation effects at high  $\gamma$ -doses .*

## I. AEROGEL FABRICATION, SURFACING, AND COATING

### Aerogel Fabrication

Silica aerogel materials were fabricated by both the high temperature and low temperature methods at the Lawrence Livermore National Laboratory in the Department of Chemistry and Materials Science by Tillotson and Hrubish. Tetramethoxysilane (TMOS) is partially hydrolyzed with water in methanol, in the presence of an acid catalyst (HCl) to expedite gelation. The mixture is refluxed for 15 hours and the MeOH is removed by distillation. This gives a condensed silica oil which is further hydrolyzed with H<sub>2</sub>O. The gel is condensed(solvent is extracted) by either supercritical extraction of the solvent at high pressures and temperatures or a low pressure and temperature solvent replacement process. In the latter, the solvent (usually an alcohol) is replaced by liquid CO<sub>2</sub> which is then supercritically extracted in a critical point drying unit. By condensing the gel in this way, the gel resists collapse associated with xerogels and hence maintains its volume during the drying process. This yields the highly porous structure of an open celled foam.

### Aerogel Surface Treatment

The surface of aerogel is defined by its molecular structure. Small Angle X-ray Scattering (SAXS) experiments indicate that for aerogel, with density in the low tens of milligrams per cubic centimeter, the topology is fractal in nature, with a chain-like branched polymeric structure having

randomly distributed branches. With increasing density, the structure approaches a uniform, nearly smooth surface with very small pores (of the order 5-50 angstroms for densified systems).

Just as with glass, the transmissive properties of aerogel improve with polishing. The technique for polishing the aerogel, however, is different from that of polishing glass. Since liquids dissolve the solgel material, the typical methods employed by glass engineers will fail to yield useful results. Instead of water, a freon spray was used during the lapping process. This freon spray, if over applied, causes the material to become too wet, causing condensation of liquid onto the surface of the material, which starts to dissolve the material. This problem was avoided using only a minimum amount of spray applied directly onto the lapping paper rather than onto the aerogel surface, minimizing this over-wetting effect. Dry nitrogen was also used as a "slurry" gas.

The lapping was performed on diamond lapping film with rms roughness ranging from 0.3 to 63 microns. These lapping films are generally used for polishing fiber optical cables after cleaving, and are commercially available. Figure 1 is an optical photomicrograph (65x) of a sample of aerogel of density  $450 \text{ mg-cm}^{-3}$  prior to polishing. The rough surface morphology and porosity is evident from the Figure. Figure 2 is a photomicrograph of the same sample after lapping 1 minute with a diamond lapping film having a rms roughness of 64 microns followed by 1 minute at 40 microns. The circular arc in the lower section of the sample is due to a circular lapping motion.

Figure 3 illustrates the result of applying nutating figure-eight lapping motion. The lapping program used was : 30 seconds at 40 microns, 1 minute at 15 microns, 1 minute at 9 microns, 2 minutes at 3 microns, and 3 minutes at 1 micron. These are probably not optimal lapping times however, and more work needs to be done in this area to determine the optimal procedure. The bright spots correspond to higher areas. Figure 4 is an optical micrograph of the sample of Figure 3 after treatment with a nutating figure-eight pattern lapping motion on diamond lapping paper in the following sequence: 2 minutes at 0.3 microns, 1 minute at 0.5 microns and 2 minutes at 0.3 microns. Note the uniformity of the surface which is indicated by the uniform color in the micrograph.

The data demonstrating the effectiveness of this method for improving the transmissive optical properties of  $257 \text{ mg/cc}$  aerogel material are illustrated in Figure 5, which plots the visible transmission spectra of both the polished (P), and unpolished (U) surfaces as a function of wavelength. The transmission spectra for polished aerogel samples of several densities are plotted in Figure 6. Figure 6 implies an increasing relationship between density and percent transmission in the visible spectrum for all samples except the  $83 \text{ mg/cm}^3$  density sample which inexplicably crosses the other curves. The infrared transmission spectra for these samples are shown in Figure 7 and, as in Figure 4, indicates an increasing relationship between density and transmittance. In the infrared energy regime, the  $83 \text{ mg/cc}$  sample's transmittance does not cross the other curves as in the visible. The deep wells in Figure 7 have a frequency response which correlates with  $\text{H}_2\text{O}$  and  $\text{CO}_2$  absorption bands, and are expected in a highly porous system such as aerogel which has been at ambient conditions for several weeks.

Figure 8 is a SEM micrograph (magnification 30Kx) of a sample of  $349 \text{ mg/cc}$  aerogel prior to polishing. Notice the deep voids. Figure 9 is a SEM micrograph (magnification 30.4Kx) after polishing with a similar the procedure to that described above. It is also worth noting that the aerogel may be cleaved prior to planarization rather than polished. Another way to achieve near-optical quality surfaces with aerogel would be to use a very precise mold. For example, the LODTM (large optical diamond turning machine) at the LLNL would be a good candidate for fabricating a solgel mold with single or low tens of angstrom rms roughness. The resulting aerogel surface could then be very complex (e.g., aspherical) and of very high quality requiring

only the application of coatings for the finished product, rather than polishing and machining followed by planarization and coating. The LLNL group has also reported the use of a higher density aerogel to polish the test sample (of lower density)<sup>2</sup>.

### Dielectric and Metallic Coatings

PECVD (Plasma Enhanced Chemical Vapor Deposition) and thermal evaporation techniques were used to planarize the silica aerogel with SiO<sub>2</sub> prior to metalization. The PECVD was performed at the Cornell University NNF in a Technics Series 900 RF reactor using a Silane/Nitrous Oxide plasma. The substrate temperature was 240 C and RF power was 34 Watts. The film deposition rate was determined by post deposition ellipsometric measurements to be 506 angstroms/minute. An Edwards thermal evaporator was also used to deposit the SiO<sub>2</sub> planarization layer. Typically, the initial chamber pressure was  $8 \times 10^{-7}$  mbar. The substrate temperature was approximately 50-110 C (as measured by a thermocouple within 1 cm of the substrate). The evaporant was outgassed at a current of 15 amps for over 2 minutes prior to deposition. When performing both the PECVD and thermal evaporation, the substrate was outgassed under high vacuum for more than 30 minutes.

Both metallic and dielectric thin films were applied to the planarized aerogel samples. Metallic Aluminum and MLD (Multi Layer Dielectric) Al<sub>2</sub>O<sub>3</sub>/Y<sub>2</sub>O<sub>3</sub> thin films were deposited as single layer or multi-layer films. MLD coatings are of interest to the optics community for a variety of applications including highly reflective optics. Thus, the ability to apply MLD coatings to the aerogel surface is an important result, although more work should be done in the area such as sputtering of MLD films onto aerogel.

Unfortunately, at the time of this work, the QCM (quartz crystal microbalance) and optical thickness monitors were not installed into the vacuum evaporator used, so the thickness of the thin films was not measured in-situ.

*The important result however, is that for the first time, reflective surfaces were deposited onto a planarized aerogel surface which was thought to be very difficult, if not impossible.*

As stated above, dielectric planarization of polished aerogel surfaces yields a surface which is able to be coated with reflecting films. Figure 10 is a SEM photomicrograph (magnification 456x) of the cross section of a sample of 450 mg-cm<sup>-3</sup> density aerogel polished using the procedure above after the application of an SiO<sub>2</sub> planarization layer and an aluminum thin film. Viewed under an optical microscope, the sample surface appeared to have a surface roughness similar to that of the sample of Figure 4 before application of the SiO<sub>2</sub> planarization layer. The aluminum film was found to have a reflectivity of 80 percent at the "sweet spot" when measured at 632 nm at the specular angle. The lowest reflectivity measured on this sample was 40 percent. Figure 11 is a SEM micrograph (magnification 12.3Kx) of the edge of an Al film on planarized aerogel. The Figure illustrates the nature of the planarized aerogel surface in the foreground and the Al metalization layer rises vertically. The figure illustrates the ability of the polishing/planarization procedure to yield a surface suitable for reflective substrate applications (the obscuration in the foreground due to two large dust charged particles). The adhesion of the films was found acceptable using the "tape pull test"<sup>4</sup> in which a piece of Scotch tape is allowed to come to rest on the film, and after removing the tape, the integrity of the film is examined using optical and scanning electron microscopy.

The optical quality of the resulting mirrors was tested on a simple reflectometer built in the RL Photonics Laboratory. A block diagram of this device system is shown in Figure 12, and operated at 632.8 nm (HeNe laser wavelengths) for visible measurements. Typical hemispherical

scatter results for the first reflective surface are illustrated in Figure 13. This scatter data characterizes the spatial distribution of scattered light energy from the specular angle. The relative intensity is plotted as a function of scatter angle for a MLD reflector. An ideal mirror would have approximately a delta function response falling off from the angle of incidence (zero degrees). The scatter data from this prototype mirror suggests that it may be possible to fabricate a mirror using an aerogel substrate. Figure 14 illustrates the first three aerogel mirrors produced by RL (then RADC) sitting in front of two bars of  $100 \text{ mg-cm}^{-3}$  density aerogel. From left to right, the aerogel substrates had density  $350 \text{ mg-cm}^{-3}$ ,  $450 \text{ mg-cm}^{-3}$ , and  $275 \text{ mg-cm}^{-3}$ .

It may also be possible to perform a fusion of two solgel technologies to produce a better ultra-lightweight reflector. These two technologies are XEROGEL<sup>5</sup> and AEROGEL, and would work in harmony as follows: The aerogel would be diamond turned or cast to form the desired surface. Of course, this surface would be too porous for reflective optics, but to planarize the surface, utilize the XEROGEL process by spin coating the aerogel with an atomized sol and heat treating or low temperature drying the thin film under controlled pressures and temperatures. Of course, this would be complicated by the fact that XEROGELS crack and reduce their volume under drying conditions. The recent work at Sandia Labs<sup>6</sup> suggests, however, that a critical thickness of the thin film exists which minimizes cracking. It may be of interest to attempt this XEROGEL experiment using films thinner than this critical thickness.

## II. RADIATION EFFECTS IN AEROGELS

### II.I Introduction

All space optical systems must survive the radiation dose bestowed upon them by the natural space environment over their mission lifetimes. Certain military satellites have the added requirement of surviving prompt and delayed effects of high energy radiation from high altitude nuclear detonations. Although these radiation sources differ greatly in their spectral and temporal energy content, the physical mechanism of concern is the interaction of radiation with materials comprising the system. If aerogel is to be considered as a potential substrate material for space optical systems, then the effects of such radiation upon aerogel must be known. It is quite remarkable to note that :

*The aerogel samples tested as both bulk material and reflective heterostructures showed no radiation induced metastability up to 35 Mrad  $\gamma$ -ray total dose. Further, there was a correlation between the Infrared transmission and the density of paramagnetic states.*

The radiation may be particle-like (e.g.,  $\alpha$ ,  $\beta$ , p, n, e<sup>-</sup>, e<sup>+</sup>) or photonic (x-, or  $\gamma$ -ray) in nature. Although the energy of such high energy radiation greatly exceeds the binding energy for the electrons to nuclei in the structure, the physical reaction of these species with the absorbing medium varies distinctly. In this work for example, the pulsed electrons had very little measurable effect while x- and  $\gamma$ -rays produced an increase in the density of localized defect states and for higher dose rates, a corresponding decrease in IR and UV/Vis transmission (color center formation). This difference being attributed to differing scattering cross sections (or penetration depths) for these species. Electrons are known to be very strongly surface absorbed as opposed to x- or  $\gamma$ -rays, hence having lower interaction volume in the material than their photonic counterparts. This lower interaction volume, considered with the low density of the aerogel is attributed to the lack of a significant electron induced radiation effect measurement. Details of the experiment appear in the next section.



In the process of traversing the sample volume, these high energy species give up their energy to absorber atoms creating defects such as: ionized atoms, free electrons, electron-positron pairs, displaced nuclei, dangling bonds, strained bonds, disclinations, dislocations, further elementary excitations of defect centers, and secondary and tertiary scattering effects. The effects of these defects upon optical elements include changes in mechanical and electro-optical properties (e.g. internal stress and strain tensors, density, Electro-optic coefficient, dielectric constant, charge separation). The mechanical changes correspond to surface deformation which destroys optical wave front integrity. Color centers decrease optical transmission, and serve as sites for space charge buildup. Changes in optical absorption correspond to increased absorption of laser radiation potentially leading to sub-optimal optical train operation. This section is a simplified review of radiation induced defect dynamics in amorphous silica and reports results of preliminary studies the author performed on the interaction of electron, x- and  $\gamma$ -ray radiation with (coated and uncoated) aerogel materials.

### Absorption Physics

There are three processes responsible for photonic radiation absorption: *photoelectric absorption* ( $\tau(E)$ ), *Compton scattering* ( $\sigma(E)$ ), and *electron-positron pair formation* ( $\kappa(E)$ ). The probability of these processes occurring is expressed quantum mechanically as a scattering cross section, or absorption coefficient  $\mu(E)$ . This can be written as the sum of the probabilities of these processes:  $\mu = \tau + \sigma + \kappa$ ; Where  $\rho$  is the density of the material,  $N$  is an Avogadro's number of atoms,  $Z$  is the atomic number, and  $A$  is the atomic weight. In the photoelectric process, incident photon energy ( $h\nu$ ) is absorbed by a *bound* electron which is ejected from the atom with kinetic energy  $T = h\nu - \phi$ ; where  $\phi$  is the ionization potential of the electron. This electron may be adsorbed by the absorber at a defect state or ejected from the absorber.  $\tau(E)$  dominates  $\mu(E)$  at low energies (less than  $\approx 200$  KeV).  $\tau(E)$  varies as  $Z^4$  and  $(h\nu)^{-3/2}$ . This dependence illustrates the fact that  $\tau$  is dependent on material density and incident photon energy. As the energy increases, Compton scattering  $\sigma(E)$  replaces  $\tau(E)$  as the dominant term in  $\mu(E)$ . Here, the incident photon energy is adsorbed by the scattering atom inducing ionization, ejecting an electron and the atom radiates a photon at a lower energy.  $\sigma(E)$ , is proportional to  $Z$  and  $(h\nu)^{-1}$ , since each electron scatters incident photons independently. Again, the importance of low  $Z$  materials for use in high energy environments requiring minimal radiation effects is implied. At high enough energies, both  $\tau(E)$  and  $\sigma(E)$  are negligible compared to  $\kappa(E)$ . The interaction of the incident photon with energy  $h\nu > 2m_0c^2$  (1.02 MeV) raises an electron from a  $|-\rangle$  state to a  $|+\rangle$  state accordance with the Dirac Equation, creating an  $e^+ - e^-$  pair. The recoil energy from the process is taken up in the Coulomb field of the nucleus.  $\kappa(E)$  is proportional to  $Z^2$ , which like  $\tau(E)$  increases quickly with atomic number for a given incident  $h\nu$ .

### Defect Physics

Silica aerogel is an amorphous  $\text{SiO}_2$  matrix of high porosity (or a low density disordered material). The amorphous nature of the aerogel structure gives rise to a lack of translational invariance and a non-zero electronic density of bandgap states associated with localized defects. This of course differs from crystalline quartz "glass" which has the translational invariance and coordination statistics associated with a very low localized defect density (less than  $10^{15} \text{cm}^{-3}$ ). The density of quartz, however, is a factor of six greater than that of the aerogel used herein. From absorption section above, it is clear that this density yields a higher radiation scattering cross section (or defect creation probability) for quartz than for aerogel.

As the sample is presented with a high energy radiation flux, a Si-Si bond or Si-O bond may be broken creating a defect state. There are many pathologies that may be considered possible

for the resulting defect (Si dangling bond with zero to three oxygen back bonds, atomic oxygen, hydrogen dangling bonds, or Si-H). These defect centers may be neutral or charged, and thus may or may not be paramagnetic. If the centers are paramagnetic then they are detectable by standard Electron Paramagnetic Resonance (EPR). EPR measures the interaction of the magnetic moment of a paramagnetic entity (e.g.  $|↑\rangle$ ) with an externally applied magnetic field. This interaction energy is related to the cardinality of spin system, thereby allowing enumeration of the paramagnetic defect density in the sample. Even theoretically, EPR is not able to determine the *true* spin density in the system due to the existence of non-paramagnetic defect states. Charges liberated in the interaction process may further become trapped at energetically favorable defect centers changing their character to non-paramagnetic. An example of such an interaction is:

$|D^0\rangle + h\nu \Rightarrow |D^+\rangle$  in which a neutral dangling bond's electronic wave function is de-localized by absorption of an incident photon's energy. The author has investigated Light induced ESR (LESr) as an electron double resonance spectroscopic technique for enumeration of non-paramagnetic defects in other disordered systems, but this was not performed in this work, which considers only paramagnetic electronic defect states (henceforth *D-center*) in aerogels. The analysis proceeds below: The spin state of the D-center is expressed by the spin Hamiltonian<sup>9</sup>:

$$H = \underbrace{g_0 \mu_B \vec{H}_0 \cdot \vec{S}}_1 + \underbrace{\mu_B \vec{H}_0 \cdot \delta \vec{g} \cdot \vec{S}}_2 + \underbrace{\vec{I} \cdot \vec{A} \cdot \vec{S}}_3 + \underbrace{\vec{S}_i \cdot \vec{D} \cdot \vec{S}_j}_4$$

Here  $g_0 (=2.0023193)$  is the Lande-Factor of the free electron state,  $\mu_B$  is the Bohr magneton

$$\mu_B = \frac{eh}{2\pi mc} = 9.274096 \times 10^{-24} \text{ J/T} ,$$

$\vec{H}_0$  is the applied magnetic field,  $\vec{S}$  and  $\vec{I}$  are the electron and nuclear spin operators,  $\delta \vec{g}$  is the spin orbit coupling interaction tensor,  $\vec{A}$  is the hyperfine interaction tensor, and  $\vec{D}$  is the spin-spin coupling interaction tensor. The first term is the Zeeman energy of a free electron with magnetic moment ( $\mu_e = g_0 \mu_B \vec{S}$ ). This term defines the external field as the direction of quantization. The defect physics manifests itself through the last three terms as perturbations. The condition for resonance is  $h\nu = \langle m_s | H | m_s \rangle - \langle m_s | H | m_s - 1 \rangle = g_s \mu_B H_0$ , ( $m_s$  is the electron spin quantum number) which for, this case is in the microwave energy range. The second term is the same as the Zeeman term except the  $\delta \vec{g}$  tensor replaces the scalar  $g_0$ . This term expresses the g-shift observed in the radiated samples. The components of  $g_0$  are :

$$\delta g = -2 \sum_{n \neq 0} \frac{\langle \delta_0 | V_{so} L_i | n \rangle \langle n | L_j | \delta_0 \rangle}{E_n - E_{\delta_0}}$$

Here,  $|\delta_0\rangle$  is the ground state of the defect, and  $|n\rangle$  is an arbitrary state,  $V_{so}$  is the potential of the spin orbit term, and  $\vec{L}$  is the orbital angular momentum. The third term is the hyperfine splitting caused by the interaction of nuclear spins  $\vec{I}$  with  $\vec{S}$ . The hyperfine interaction tensor has isotropic and anisotropic components corresponding to s-like electrons and p- or d- like electrons.

$$\bar{A}_{iso} = (\frac{8\pi}{3})g_e\mu_B g_n\mu_n |\Psi(0)|^2 \bar{\delta}_{ij}, \text{ where } \bar{\delta}_{ij}$$

is the unit tensor as would be expected for an s-like wave function. The Anisotropic components of the hyperfine tensor yield the dipole-dipole interaction for p- and d-like wave functions:

$$\bar{A}_{aniso} = g_e\mu_B g_n\mu_n \langle r^{-3} \rangle \left( \langle \frac{3x_i x_j}{r^2} \rangle - \delta_{ij} \right)$$

The fourth term gives the spin-spin interaction term. This term is generally considered unimportant for systems with less than  $10^{19}$  spins  $\text{cm}^{-3}$  but in high energy radiation damaged systems it is possible to introduce a topologically one- dimensional disclination type defect. This entity would have potential for spin-spin dipole interactions-- even at low overall defect densities.

## II.II Experimental

### Sample Irradiation

As described above, two populations of aerogel samples were treated with varied doses of electrons, x- and  $\gamma$ -rays. The first sample type was bulk unpolished silica aerogel of density  $347 \text{ mg/cm}^3$ . These samples were cut into bars with square cross section ( $0.6 \text{ cm} \times 0.6 \text{ cm} \pm .5 \text{ mm}$ ) for calibrated transmission and absorption measurement within the sample family. The second family of samples of aerogel consisted of polished,  $\text{SiO}_2$ -planarized aerogel (density =  $450 \text{ mg/cm}^3$ ) coated with a reflective aluminum thin film. Table 2.1 gives the details of the sample population characteristics and irradiation treatment.

As displayed in Table 2.1, the experimental measures of radiation effects upon the bulk aerogel samples were EPR and transmission mode Fourier Transform-Infrared (FT-IR) and UV/Vis spectrophotometry. For the coated samples, FT-IR reflection mode spectrophotometry was used.

Figure 15 shows the UV/Vis transmission spectra for the bulk aerogel samples subjected to 10 Mrad of gamma ray irradiation. The dose rate was 2 Mrad/hour with a temperature of approximately 80 C at the samples. There was no visible evidence of aerogel photo darkening while the co-treated Corning 7059 glass slide appeared brown in color. The visible spectra showed no change in transmittance, as illustrated in the Figure. The IR transmission likewise showed no notable change. The IR reflection spectra for the coated aerogel samples are shown in Figure 16 (R refers to radiated sample). These curves are essentially flat across wavelengths from two to five microns, except for the presence of  $\text{H}_2\text{O}$  and  $\text{CO}_2$  absorption bands. These samples received 35 Mrad of gamma radiation. Figure 17 is a plot of the EPR-measured defect density (Si dangling bond signature) for samples of bulk aerogel irradiated to a total g-ray dose of 100 Mrad (circles) and corresponding 2.35 micron FT-IR transmission peak height for these data. It is remarkable that there is negligible increase in spin density *and* no decrease in IR transmission till 35 Mrad. It is even more interesting to note the exponential correlation between these data as plotted in Figure 18. By increasing the receiver gain, the magnetic field scan range and magnetic field modulation amplitude while being careful not to be in nonlinear operating regimes (power saturation and modulation amplitude cutoff), the presence of anisotropic hyperfine satellites appeared in the samples treated with 80, 90 and 100 Mrad of gamma radiation. The cleanest signature (100 Mrad case) is illustrated in Figure 19.

### III. CONCLUSIONS

The results of a preliminary investigation of silica aerogels as a potential optical substrate material was investigated. The aerogel surface was passivated using  $\text{SiO}_2$  thin films prior to the deposition of metal films. This material is on the order of six times less dense than conventional ULE glass substrate material. This low density gives the material remarkable resistance to ionizing radiation relative to ULE and once past the radiation resistance threshold, these data seem to imply the existence of an exponential correlation between EPR paramagnetic defect density and IR absorption. The EPR data also seem to imply that four terms of the spin Hamiltonian should be considered in the analysis of radiation effects in aerogel including spin interaction which is usually unimportant for dilute spin systems such as these. The resulting ultra-lightweight of an optical element which could be fabricated from aerogel could have a substantial impact upon system weight, which translates into reduced launch and on-orbit costs. The results indicate optical reflectivity and radiation resistance of the material are optimistic, but much more research and development must occur before a realistic optic can be fabricated with this material.

## ACKNOWLEDGMENTS

This research was performed over the past 2.3 years through Air Force and SDIO support and funding. The author thanks the project management over for their support despite shrinking budgets. The research could not have been performed without the hospitality, mentor ship and advocacy of L. Hrubish, T. Tillotson, and R. Pekala of the Dept. of Chemistry and Materials Science at Lawrence Livermore National Laboratory in the fabrication of the aerogel samples. The hospitality of The National Nanofabrication Facility at Cornell University is gratefully acknowledged for the use of PECVD and thin film characterization apparatus. The hospitality of Syracuse University for the author's use of an EPR spectrometer is gratefully acknowledged. The author is grateful to H. Roth and staff of the Rome Laboratory (Hanscom AFB) Solid State Sciences Directorate for the use of facilities and technicians in performing sample radiation and the use of materials characterization apparatus. The donation of laboratory equipment and support of E. Blackburn and the RL Reliability Physics Branch is gratefully acknowledged. The author thanks George Allen, an RL summer student, for performing the optical reflectivity measurements.

Table 2.1 Experiment Design

INCIDENT RADIATION	SAMPLE TYPE	
	I. BULK	II. MIRROR
Electrons <sup>1</sup>	14.33 Krad	-----
X-ray <sup>1</sup>	20.0 rad	-----
$\gamma$ -ray <sup>2</sup>	0-100 Mrad	0-100 Mrad

1: Electron Source: Linear Accelerator at Rome Laboratory (Hanscom AFB) dose rate :  $2.17 \times 10^{10}$  rad/sec. X-rays generated by focusing LINAC beam on a Bremsstrahlung target. X-ray dose rate:  $1.56 \times 10^8$  rad/sec. Total dose measured by PIN diode and TLD techniques.

2: Gamma Ray Source:  $^{60}\text{Co}$  with dose rate of 2 Mrad/hr. Total dose measured by calorimeter.

## References

1. S.S. Kistler, J. Phys. Chem. 36, 52 (1932).
2. L. W. Hrubiesh, T.M. Tillotson , LLNL private communication (1990).
3. R. Bussjager and J. Maurice of the RADC PHOTONICS LABORATORY, suggested the use of a NEWPORT fiber microscope for the observation of surface quality during the polishing steps.
4. S. Wolf and R.N. Tauber, *Silicon Processing for the VLSI ERA*, Vol. 1 Process Technology (Lattice Press, 1986).
5. C.J. Brinker and G.W. Scherer, *Sol-Gel Science*, (Academic Press, 1990).
6. C.J. Brinker, Proc. SOLGEL Thin Film Workshop, Sandia National Laboratory (1990).
7. D.W. Shaefer, and K.D. Keefer, Structure of Random Porous Materials: Silica Aerogel, Phys. Rev. Lett. 56, no. 20, 2199-2202, (1986).
8. E.J. Frieble, et.al., Radiation Effects on Low Expansion Coefficient Glasses and Ceramics, in Proc. High Power Optical Components Conf. (NWC TP-7080, 30 Oct. 1986).
9. C.P. Slichter, *Principles of Magnetic Resonance*, Harper and Row, New York (1963).
10. S. Yamasaki, et. al.,  $^1\text{H}$  electron-Nuclear-Double-Resonance Detected ESR of Light Soaked a-Si:H, Phys. Rev. B, 35, no.12, 6471, (1987).

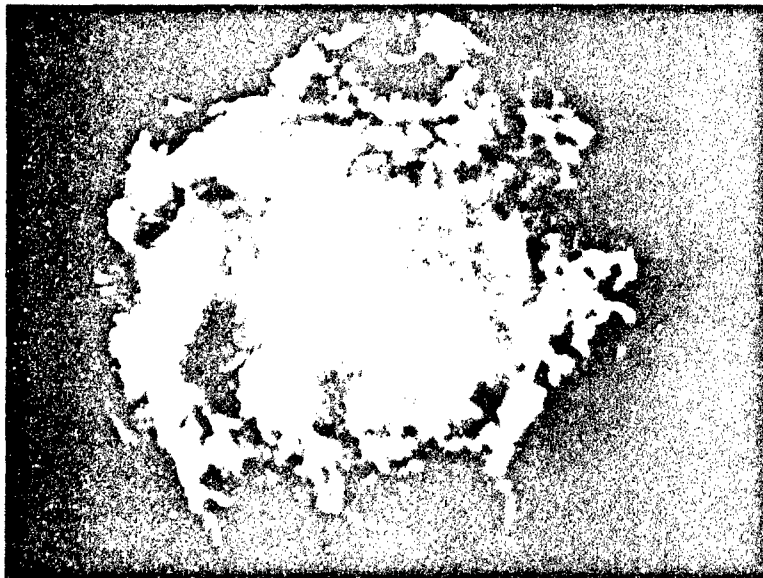


Figure 1 An optical photomicrograph of a sample of aerogel with density of 450 mg/cc. The magnification used was 65x, the bar corresponds to 80 microns. Note the uneven surface topography and a high porosity.

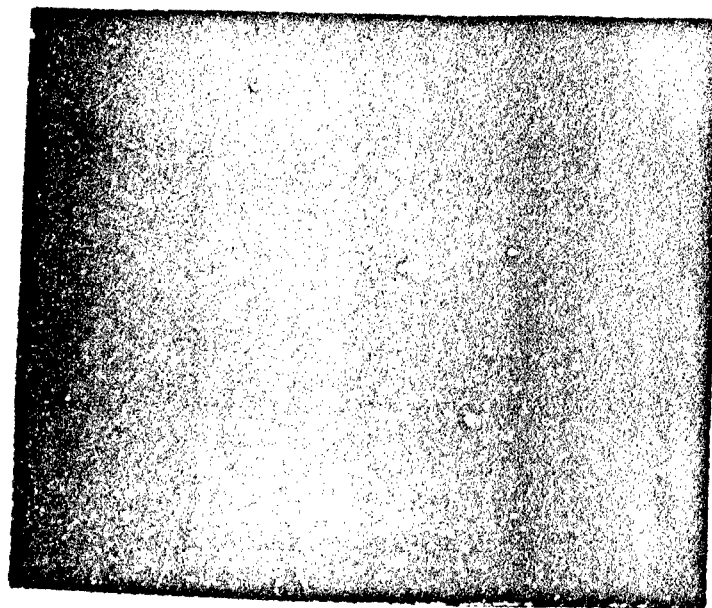


Figure 2 Optical micrograph of the sample shown in Figure 1 after polishing with a circular polishing stroke. Note the circular arc at the bottom of the figure. This defect was attributed to the lapping motion. The diamond Lapping paper roughness is 68 microns.



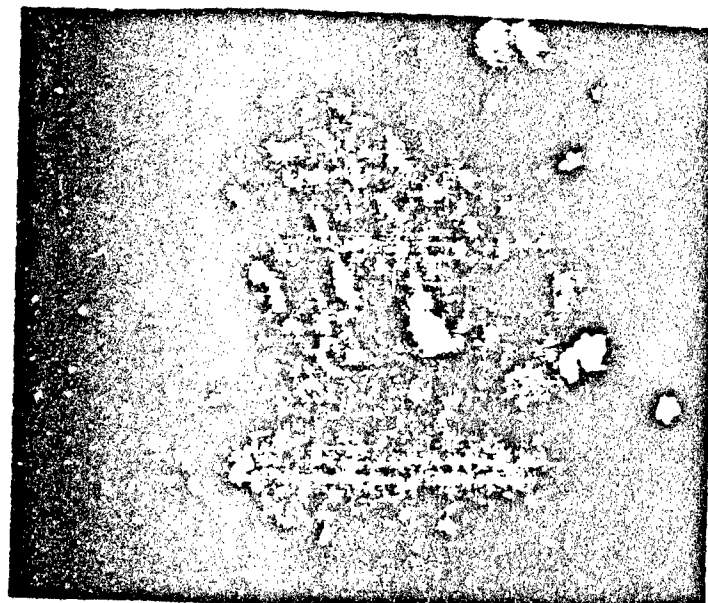


Figure 3 Optical micrograph of the sample of figure 2 after lapping with a nutating figure-eight lapping motion. The bright spots correspond to higher areas. The rms roughness of the diamond lapping film used was varied from 40 microns to 1 micron in the time sequence: 30 seconds @40, 1 minute @ 15, 1 minute @9, 2 minutes @3, and 3 minutes @ 1 micron. These are probably not optimal lapping times however, and more work needs to be done in this area to determine optimal procedure.

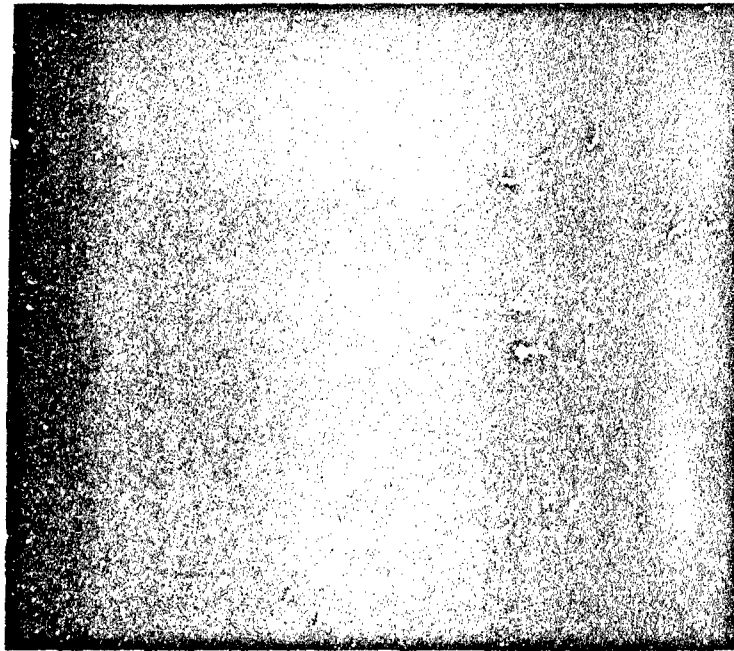


Figure 4 Optical micrograph of the sample of figure 3 after treatment with a rotating figure-eight pattern lapping motion on diamond lapping paper in the following sequence: 2 minutes @ 0.3 microns, 1 minute @ 0.5 microns and 2 minutes @ 0.3 microns. Note the uniformity of the surface which is apparent from the uniform color in the micrograph.

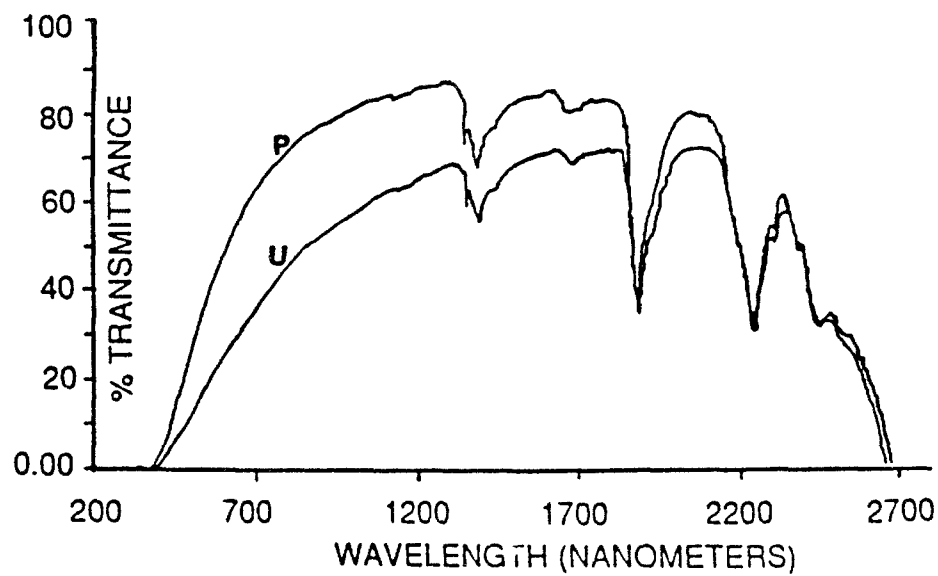


Figure 5 The effect of polishing upon aerogel UV/V is transmittance.  
P: Polished and U: as received, unpolished.

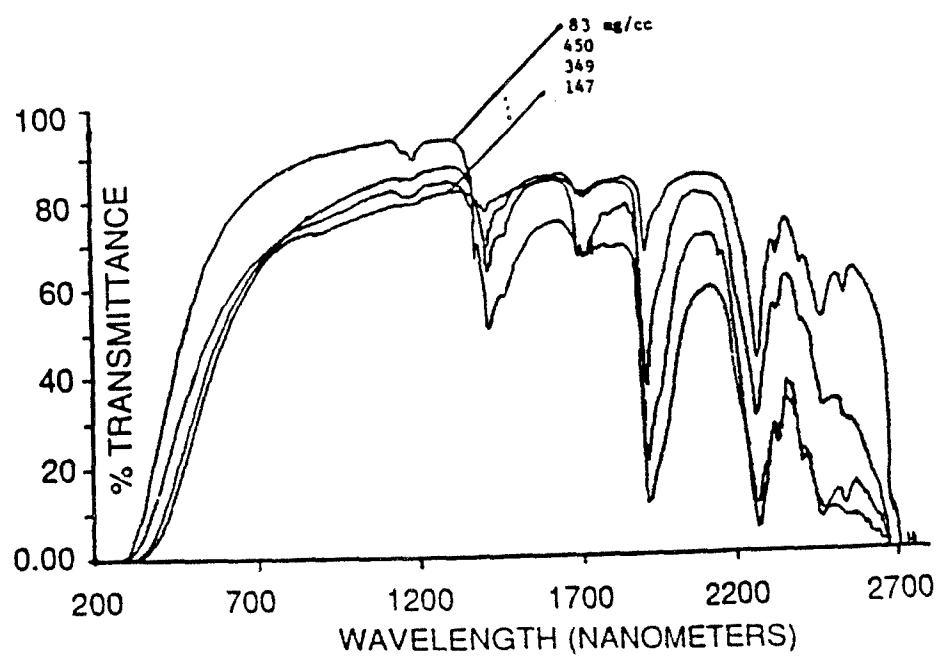


Figure 6 The UV/Vis transmittance of areogel of varied density.

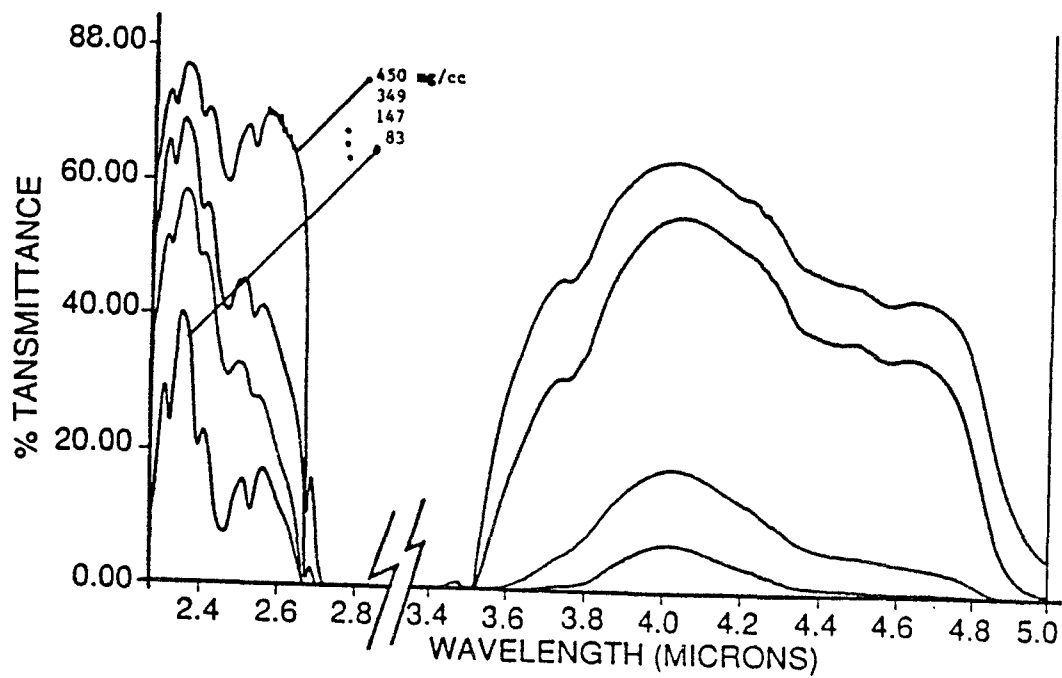


Figure 7 The IR Transmittance of aerogel of varied density.

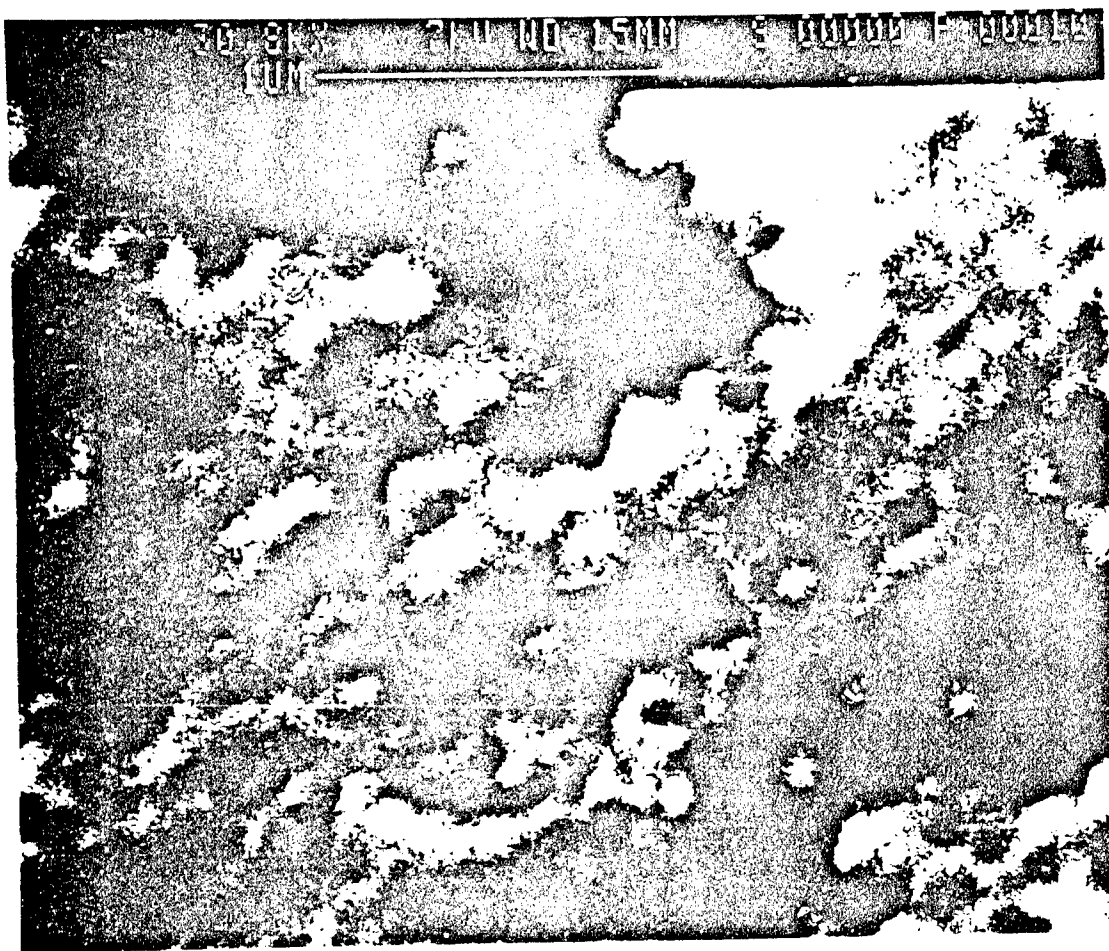


Figure 8. A SEM micrograph of 349 mg/cc aerogel prior to polishing. This sample has a relatively smooth surface. The magnification is 30 K x.

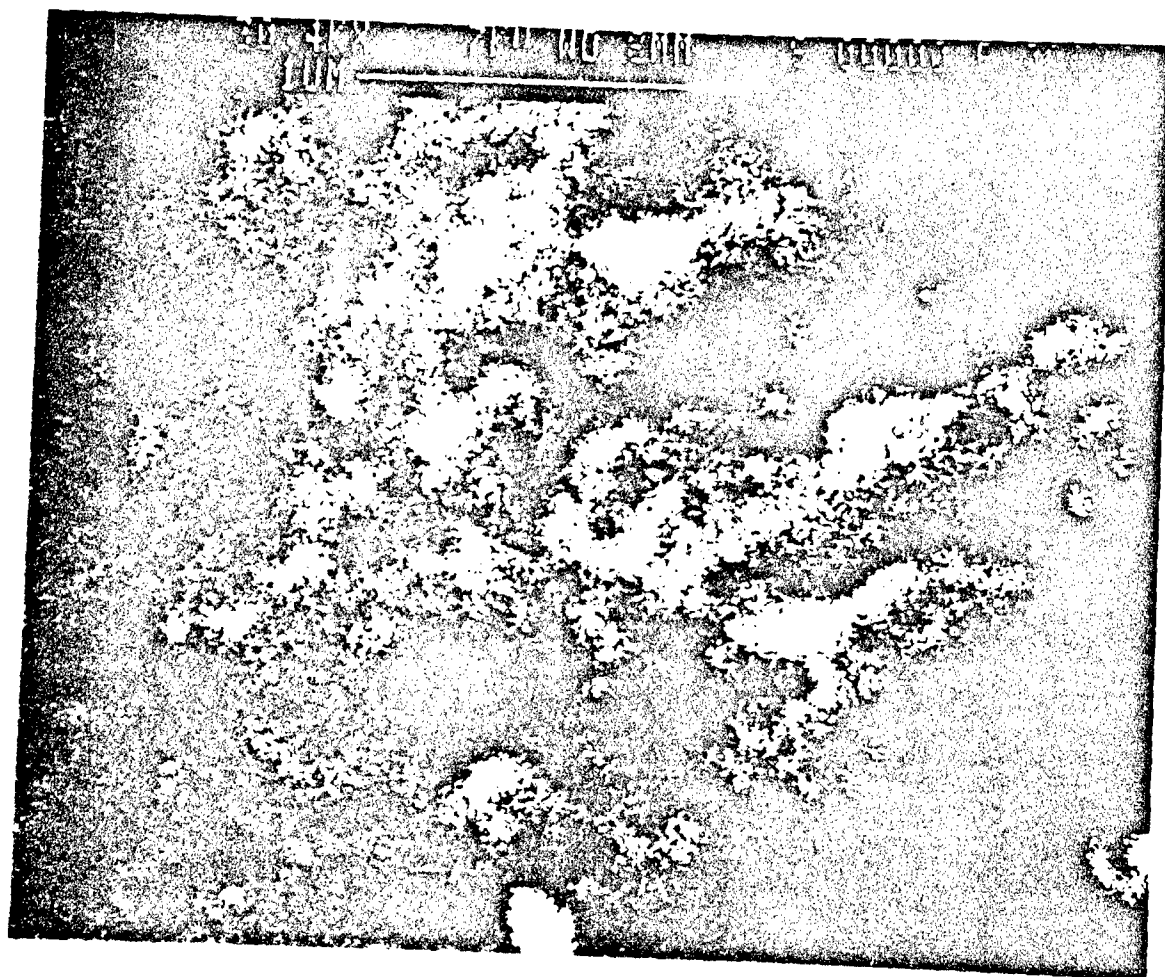


Figure 9 A SEM micrograph of the sample of figure 8 after polishing.



Figure 10 A cross-section SEM micrograph of the surface of the device which has been planarized with  $\text{SiO}_2$ .



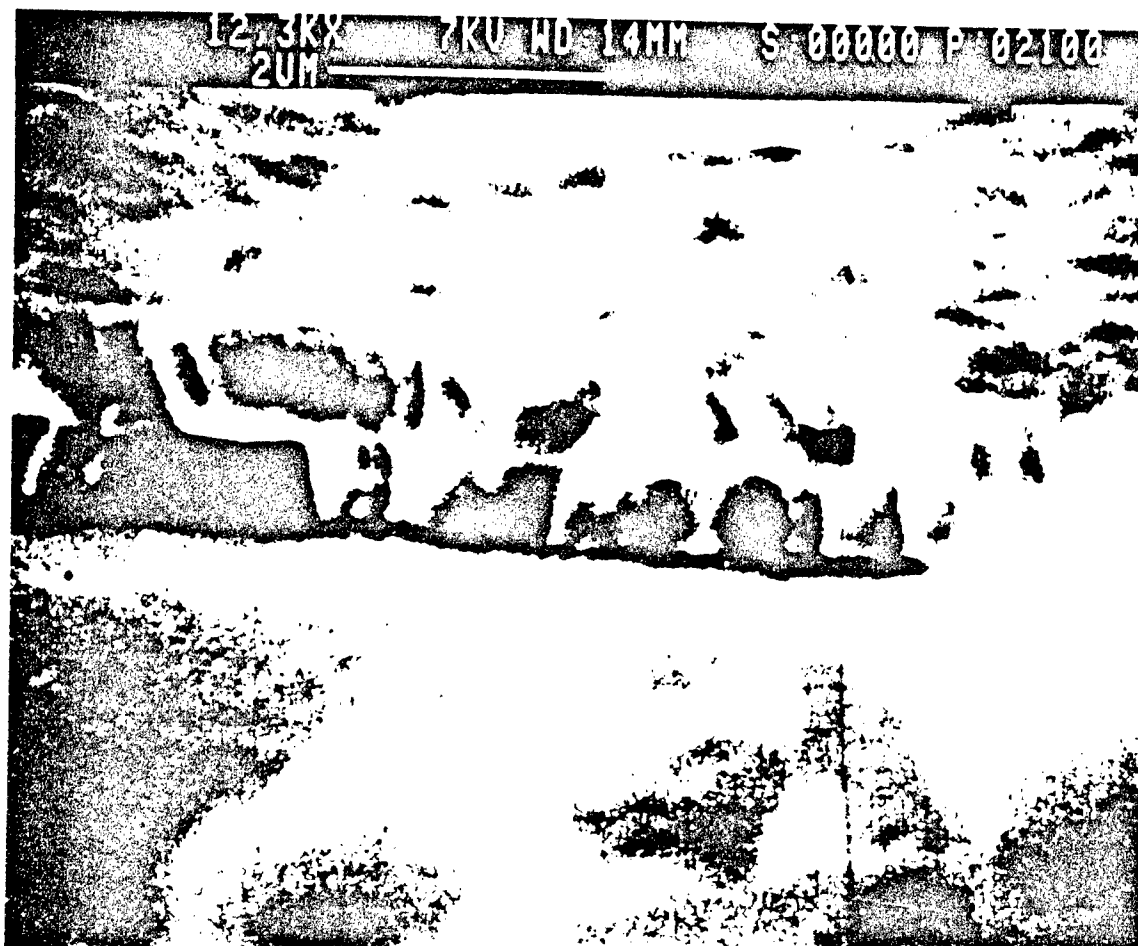


Figure 11 A SEM micrograph of an Al coating on SiO<sub>2</sub> planarized aerogel.

100

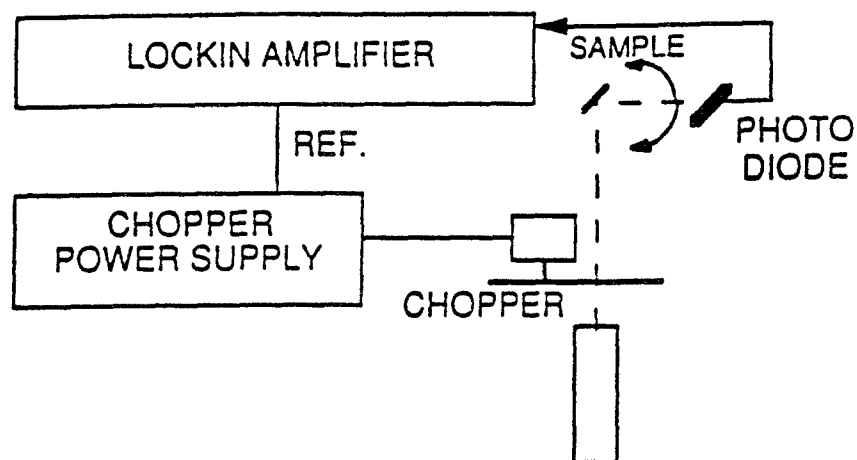


Figure 13 A block diagram of the reflectometer used to obtain optical scatter data on the samples.

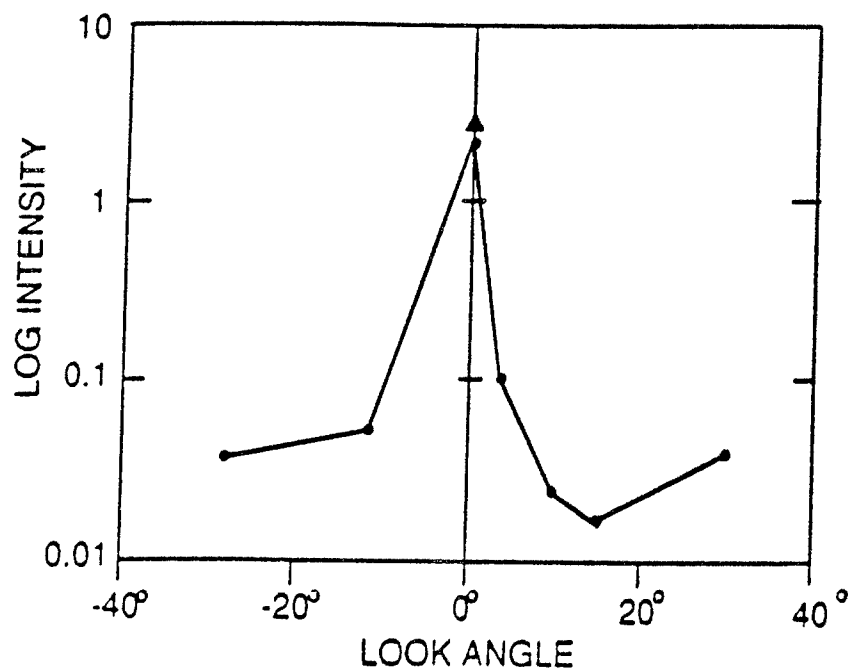


Figure 14 Typical optical scatter data for the aerogel mirrors produced to date. The triangle corresponds to the input intensity.

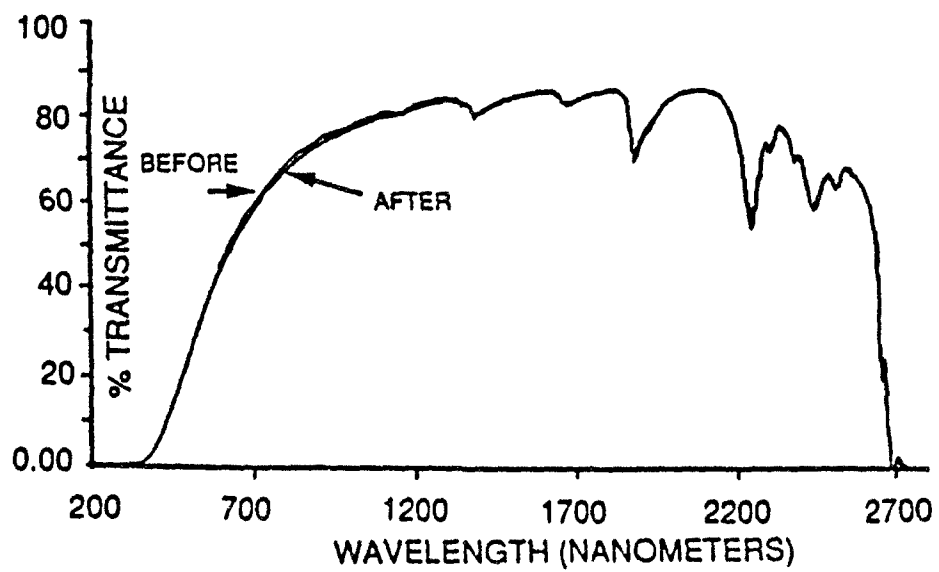


Figure 15 The UV/Vis transmission spectra for a sample of aerogel before and after treatment with 10 Mrad gamma rays.

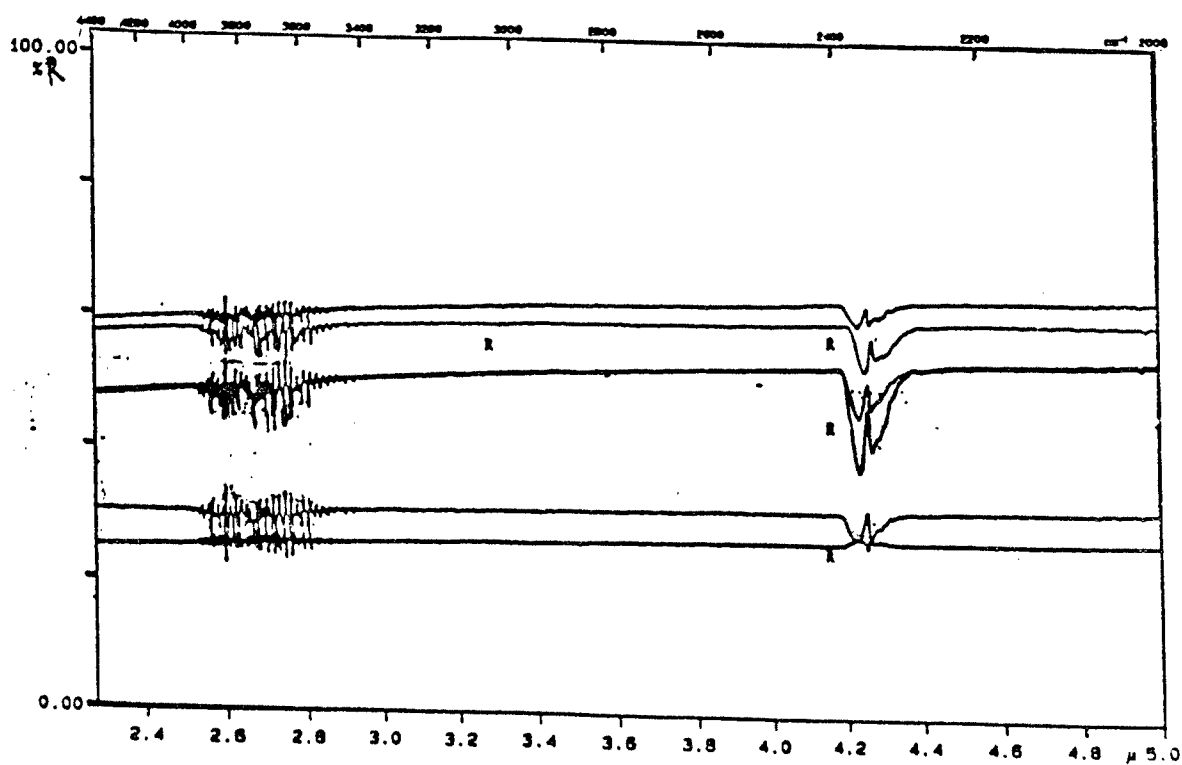


Figure 16 IR reflectivities measured on reflector samples after irradiation with 35 Mrad gamma ray irradiation.

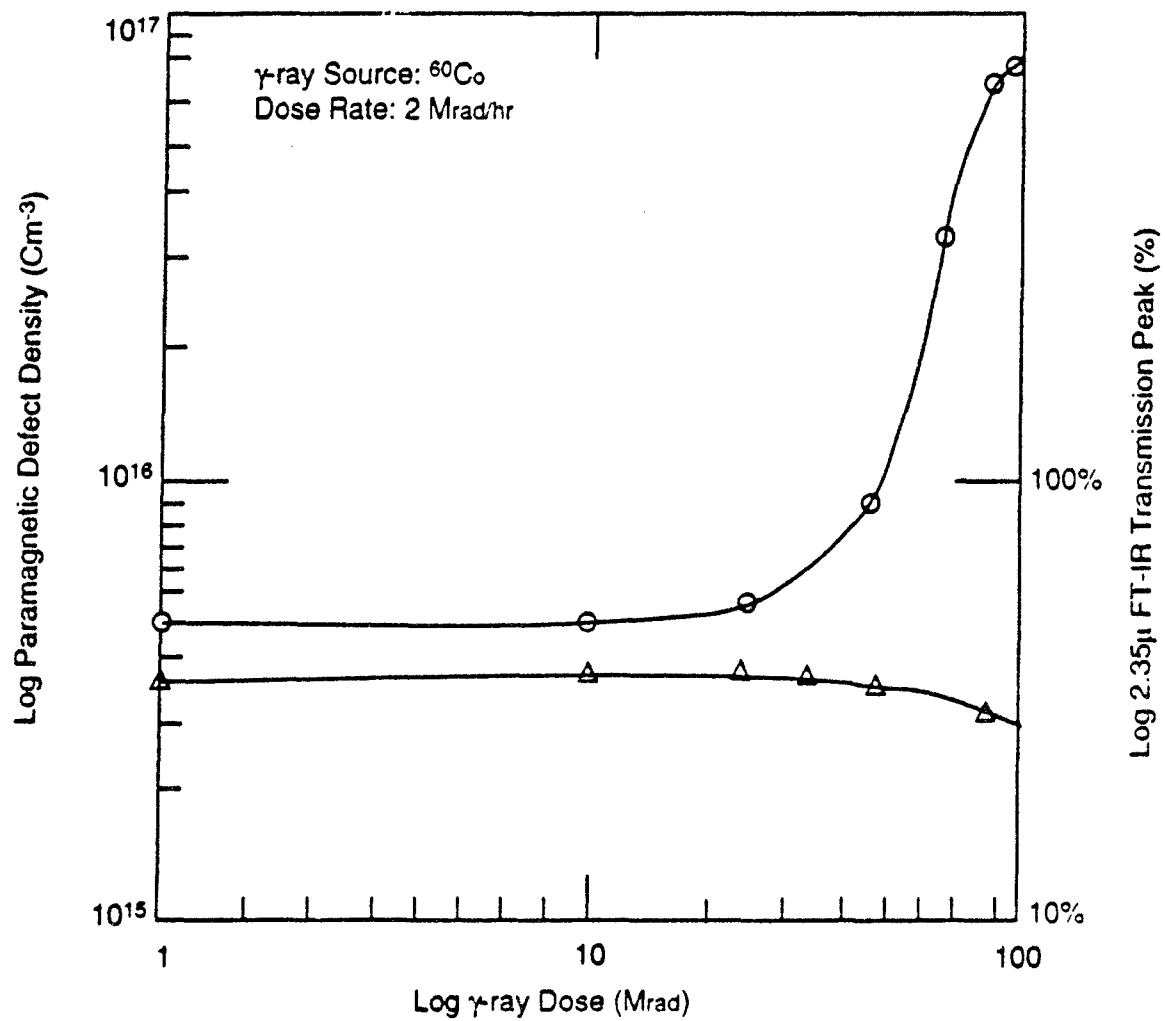


Figure 17 The paramagnetic defect density (circles) and the IR transmission of the 2.35 micron transmission peak (triangles) plotted versus gamma ray dose.

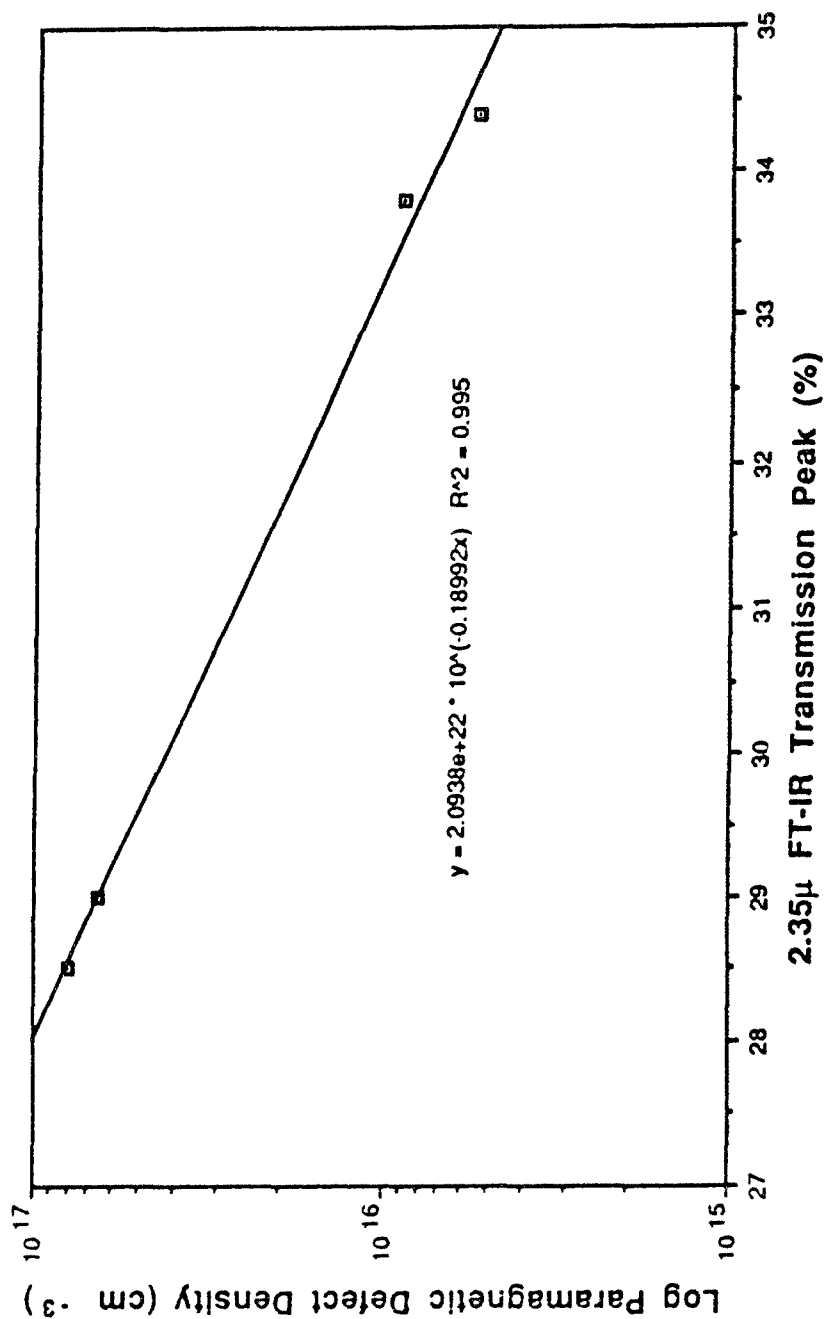


Figure 18 The exponential relation between paramagnetic defect density and the 2,35 micron FT-IR transmission peak.



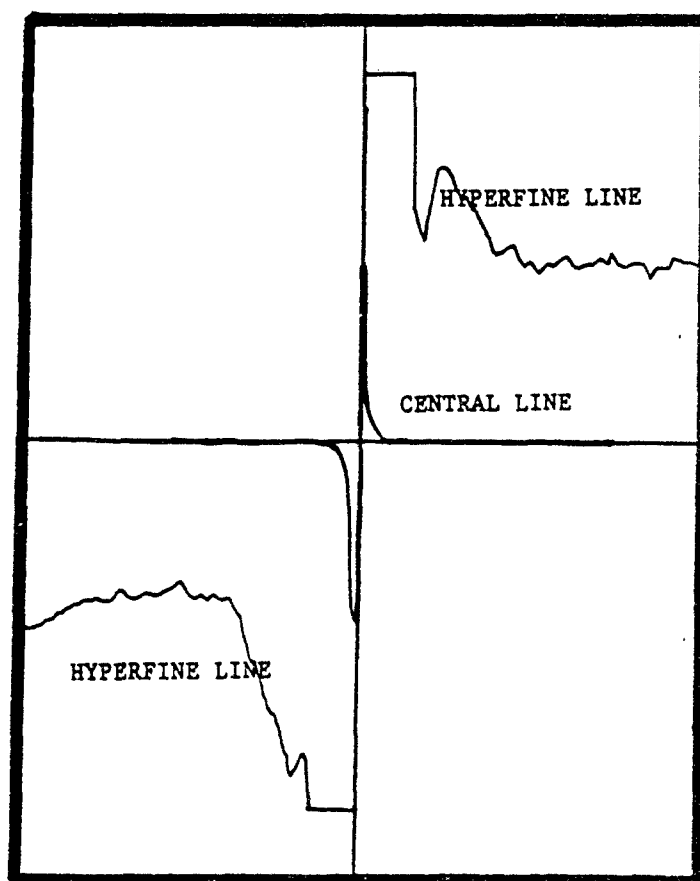


Figure 19 The EPR Hyperfine satellites from bulk aerogel sample after 100 mrad gamma irradiation. The anisotropic nature of these satellites is interesting, and suggests further work.

---

**MISSION  
OF  
ROME LABORATORY**

*Rome Laboratory plans and executes an interdisciplinary program in research, development, test, and technology transition in support of Air Force Command, Control, Communications and Intelligence (C<sup>3</sup>I) activities for all Air Force platforms. It also executes selected acquisition programs in several areas of expertise. Technical and engineering support within areas of competence is provided to ESD Program Offices (POs) and other ESD elements to perform effective acquisition of C<sup>3</sup>I systems. In addition, Rome Laboratory's technology supports other AFSC Product Divisions, the Air Force user community, and other DOD and non-DOD agencies. Rome Laboratory maintains technical competence and research programs in areas including, but not limited to, communications, command and control, battle management, intelligence information processing, computational sciences and software producibility, wide area surveillance/sensors, signal processing, solid state sciences, photonics, electromagnetic technology, superconductivity, and electronic reliability/maintainability and testability.*